IQ Impedance Modulator Front-End for Low-Power LoRa Backscattering Devices

Daniel Belo, Ricardo Correia, Yuan Ding, Spyridon N. Daskalakis, George Goussetis, Apostolos Georgiadis, and Nuno Borges Carvalho

***Abstract*—This paper describes the design of an IQ impedance modulator radio front-end which is used to generate Long Range (LoRa) symbols with backscattering techniques, allowing to build low-power devices that may be compatible with the current LoRa networks. It is shown that a linear frequency modulated chirp can be generated by properly varying the phase of a reflected wave instead of directly varying its instantaneous frequency. The proposed device consists of two Radio Frequency (RF) transistors that generate a set of impedances by changing their gate bias, allowing to reflect their incident wave with pre-defined phase values. By joining these two reflected waves in quadrature, a new set of impedances is obtained whose phases vary 360 degrees, on a constant Voltage Standing Wave Ratio (VSWR) circle. In order to validate the proposed design, several LoRa symbols were generated and successfully transmitted and decoded. Measurements of the Bit Error Rate (BER) versus Signal-to-Noise Ratio (SNR) were conducted and shown to be in accordance with other related work. Moreover, the impact of intentional perturbations added to the control bias voltages was analyzed and tests Over-The-Air (OTA) were performed for different indoor propagation scenarios.**

***Index Terms*—Backscatter communications, chirp spread spectrum (CSS), internet of things (IoT), LoRa modulation, wireless power transfer (WPT), wireless sensor network (WSN).**

I. Introduction

IN the Internet of Things (IoT) context, where billions of connected objects are expected to be deployed worldwide, the frequent battery maintenance of these ubiquitous wireless nodes is undesirable or even impossible. The growth of the number of such devices will be possible only if the sensors' battery needs are eliminated or significantly reduced. For low power sensors and devices, careful power management and conservation are critical to the devices' lifetime and network effectiveness. One of the possible solutions is to completely change the paradigm of the radio transceivers in the wireless nodes of an IoT system.

Backscatter communications, which operates by reflecting and modulating an incident radio signal, is a promising alternative to active radios, due to their low cost, low power and low complexity implementation. In most Radio Frequency Identification (RFID) systems and passive sensors, the reader to tag communication is based on conventional Amplitude/Phase shift Keying (ASK/PSK) schemes. The work reported in [1] has shown that backscatter modulation can be extended to higher order modulation schemes, such as 4-Quadrature Amplitude Modulation (4-QAM). In [2] and [3], a 16-QAM modulator for backscatter communications was developed, which may achieve higher order modulations and simultaneously low power consumption. However, the major limitation in these backscatter modulation schemes is the short communication range. While it is possible to transfer large amounts of data, their application will be limited by the distance at which it is possible to keep a link with an acceptable Bit Error Rate (BER).

Alternatively, ambient radio waves can be used as a source to backscatter data to a receiver, eliminating the need for dedicated Radio Frequency (RF) energy sources. Several studies have shown that this technique allow battery-free backscatter devices to use the signals broadcasted by FM stations [4] , TV station [5] and Wi-Fi signals [6]. In [7] the authors presented and discussed a tag that operates with ambient FM backscatter signals while featuring high order modulation 4-PAM with a real FM station located at 34.5 Km away. The operation of a proof-of-concept prototype was demonstrated in an indoor environment with a bit rate of 345 bps and a power consumption of only 27 μW.

As it is known, backscatter communications are low power and low cost, but they are mostly limited to short ranges. Table I lists the most common technologies used in IoT applications, with their respective sensitivities and data rates. The sensitivity of the technology largely determines the range at which a device can communicate. Sigfox operates in the Ultra-High Frequency (UHF) band and uses PSK modulation to transmit data at very low data rates, thus achieving long range. Narrow-band IoT (NB-IoT) is designed for connecting a wide range of static IoT devices using current cellular communication bands and infrastructures. LoRa technology presents the lowest sensitivity [8]. Also, LoRa is the most resilient transmission scheme to both in- and out-of-band interferences. It operates based on spread spectrum communication techniques and uses Linear

Manuscript received May 3, 2019; revised July 30, 2019; accepted September 8, 2019. The work of Daniel Belo was supported by the Fundação para a Ciência e Tecnologia (F.C.T.) under Ph.D. Grant SFRH/BD/142403/2018. The work of Spyridon N. Daskalakis was supported by Lloyd's Register Foundation (LRF) and the International Consortium in Nanotechnology (ICON). (*Corresponding author: Daniel Belo*)

D. Belo, Ricardo Correia and Nuno Borges Carvalho are with Instituto de Telecomunicações, Departamento de Eletrónica, Telecomunicações e Informática, Universidade de Aveiro, Aveiro 3810-193, Portugal (e-mail: a35842@ua.pt; rjoao@ua.pt; nbcarvalho@ua.pt)

Yuan Ding, Spyridon N. Daskalakis, George Goussetis and Apostolos Georgiadis are with School of Engineering and Physical Sciences, Heriot-Watt University, Edinburgh EH14 4AS, Scotland, UK (e-mail: yuan.ding@hw.ac.uk; sd70@hw.ac.uk; g.goussetis@hw.ac.uk; apostolos.georgiadis@ieee.org)

TABLE I
IOT TECHNOLOGIES WITH SENSITIVITIES AND DATA RATES. ADAPTED FROM [14]

Technology	Sensitivity	Data Rate
LoRa	-149 dBm	18 bps - 37.5 kbps
Sigfox	-126 dBm	100 bps
NB-IoT	-129 dBm	0.6 - 250 kbps
Wi-Fi (802.11 b/g)	-95 dBm	1 - 54 Mbps
Bluetooth	-97 dBm	1 - 2 Mbps
ZigBee	-100 dBm	250 kbps
RFID	-85 dBm	40 - 640 kbps

Frequency Modulated (LFM) signals with cyclic shifts to encode information. Because of the linearity between frequency and time present in this technique, the frequencies and timing offsets between transmitter and receiver are easily eliminated allowing to build a robust communication system. The chirp's frequency sweep is equivalent to the spectral bandwidth of the signal.

The ability to synthesize transmissions compatible with Wi-Fi (802.11 b) [9], Bluetooth Low Energy (BLE) [10], [11], Zigbee [12], [13], at μW of dc power using backscatter transmissions have been presented. Through these systems, it is possible to increase existing IoT networks with additional sensing devices without the need to change current protocols. In [9], the authors created IEEE 802.11b packets using backscattering techniques and received the packets on Wi-Fi chipsets, while consuming 4 to 5 orders of magnitude lower power than existing Wi-Fi chipsets. In [11] a prototype was presented that produces a band-pass FSK modulation at 1 Mb/s, showing compatibility with the BLE advertising channels. Recent studies shown that a backscatter modulator can be compatible with LoRa standard, significantly extending the backscatter communication range, as shown in [14]. The implementation can synthesize LoRa symbols by using three cascaded switches that create eight different impedances corresponding to eight different reflected phases, which constraints the implementation in terms of scalability. Due to the unavoidable harmonic content generated, in the same work, the authors also presented a harmonic cancellation technique that fairly mitigates the problem but, however, it increases the complexity of the system. In [15], the authors reused ambient LoRa transmissions as the excitation signals, and shifted the incoming active LoRa chirp by an amount of $BW/2$ and $-BW/2$ and then joined them into a new LoRa symbol, compatible to the LoRa symbol format. This implementation is entirely dependent on LoRa communications, since it uses FSK modulation with an active LoRa chirp. Moreover, the achievable data rate is lower than the LoRa, since the design can only encode one bit per active LoRa symbol.

This manuscript is an extended version of the work presented in [16], where preliminary results of an IQ backscatter modulator shown to be able to synthesize an up-chirp, which is used in the LoRa's packets preamble. In this work, a LoRa encoder and decoder was developed in order to prove that the proposed circuit can generate any LoRa symbol, proving that it may be compatible with current LoRa gateways or networks. It is also shown that it is scalable for other types of applications due to its simple implementation and versatility for different frequencies. Measurements of the BER versus Signal-to-Noise Ratio (SNR) are provided as well as several measurements Over-The-Air (OtA) with different propagation scenarios. Additionally, the robustness of the proposed design is evaluated when the control bias voltages are corrupted with specific perturbations. The modulator consists of only two transistors and a power divider and has negligible dc power consumption. The overall dc power consumption will be determined by the processing unit, which is intended to operate in baseband and to be as low power as possible, few uW [17], ideally battery-less and wirelessly powered. This allows to integrate this technology into domains such as smart cities, precision agriculture and many other applications where backscatter is currently unfeasible due to the short covering range. By developing the system for 2.45 GHz, it is possible to use Wi-Fi or 802.15.4 devices to generate the backscatter carrier, since most of those radio transceivers provide access to a special test mode that generates an unmodulated carrier signal [18].

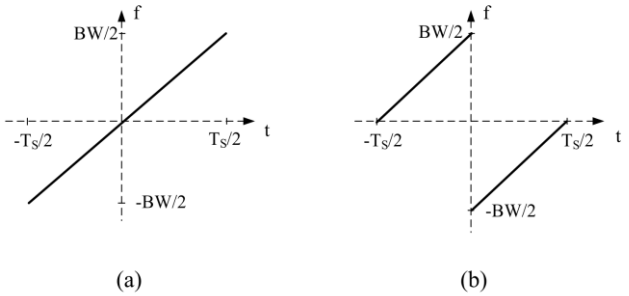

Fig. 1. LoRa symbols example. (a) Reference symbol. (b) Symbol index 64, the starting frequency is exactly in the middle of the sweeping bandwidth.

II. LORA MODULATION BASICS

This section provides an overview of the Semtech's LoRa modulation, which is used to provide long range communications. LoRa is a modulation technique based on Cirp Spread Spectrum (CSS). It uses linear frequency modulated CW signals with cyclic shifts to encode data. The bit rate achieved by such technique is given by (1),

$$R_b = SF\frac{BW}{2^{SF}}, \tag{1}$$

where SF is the spreading factor and BW is the bandwidth of the signal. The SF relates to the number of chips per symbol, namely 2^{SF} chips per symbol. Additionally, the number of bits that can be encoded within a symbol is SF. Thus, a symbol with a total length of 2^{SF} chips, can be cyclically shifted from 1 to 2^{SF} positions. The reference symbol is given by the un-shifted symbol at the beginning of a LoRa packet. The baseband reference symbol is a linear up(down)-chirp that can be represented as a complex waveform described by

$$s(t) = e^{j\phi(t)}. \tag{2}$$

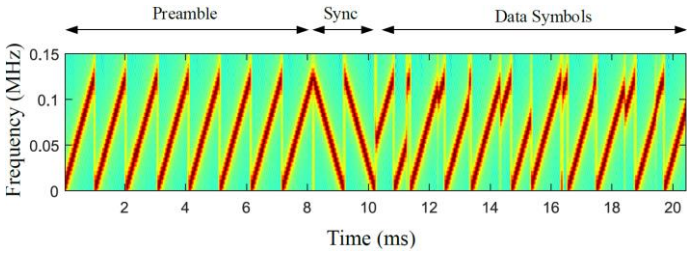

Fig. 2. Representation of a LoRa packet with SF=7 and BW=125 kHz. The packet consists of 8 preamble symbols, 2 synchronization and 10 data symbols.

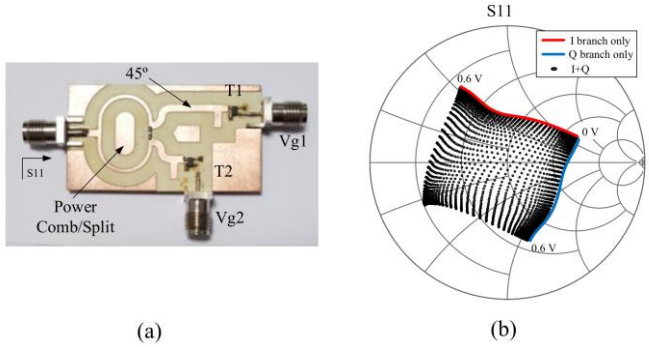

Fig. 3. IQ impedance modulator front-end. (a) Picture of the prototype. Transistor $T1$ and $T2$ are controlled by a baseband external source, such as a low power microcontroller. (b) All possible synthesized impedances measured with a grid of 10 mV step, from 0 V to 0.6 V.

The instantaneous frequency of the signal, $f(t)$, is defined as the phase changing rate given by (3).

$$f(t) = \frac{1}{2\pi}\frac{d\phi(t)}{dt} \tag{3}$$

In a linear modulated chirp, the frequency varies linearly with time. That is:

$$f(t) = \frac{BW}{T_s}t \tag{4}$$

where T_s is the LoRa symbol period given by (5) .

$$T_s = \frac{2^{SF}}{BW} \tag{5}$$

Taking into account (3), (4) and (5) and by knowing that the function for the phase is the integral of the frequency, then:

$$\phi(t) = \phi_0 + 2\pi\int_0^t f(\tau)d\tau \tag{6}$$

$$= \phi_0 + \pi\frac{BW}{T_s}t^2 \tag{7}$$

where ϕ_0 is the initial phase at the time instant $t = 0$. Based on (7) a linear modulated baseband up-chirp can be generated by properly varying the phase of a sinusoidal signal instead of directly varying its instantaneous frequency.

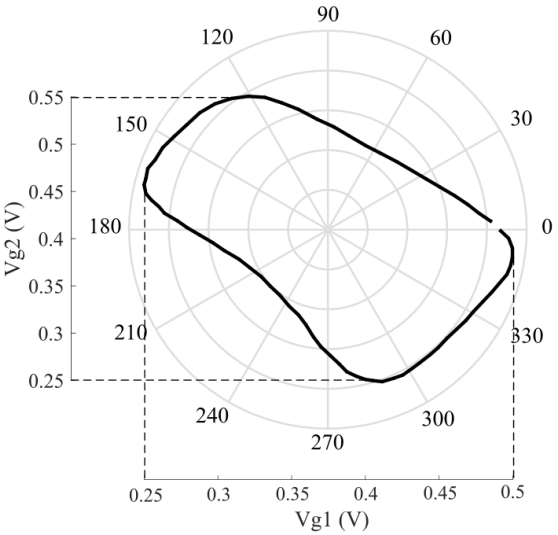

Fig. 4. Phase of the reflected wave (steps of 5 degrees) and its corresponding IQ voltages. All points will produce a reflected wave with equal amplitude.

In order to encode SF bits within an up-chirp as introduced before, LoRa uses cyclic shifts as shown in Fig. 1. The reference chirp is divided into 2^{SF} equal frequency steps and the starting frequency will represent the symbol. The transmitted symbols are detected, sampled at exactly BW Hz and multiplied by the conjugate version of the chirp used in the transmitter (up or down) as in (8).

$$z(t) = s(t)e^{-j\left(\phi_0+\pi\frac{BW}{T_s}t^2\right)} \tag{8}$$

The result is a sequence of discrete samples, $z[k = T_s/m]$, with $k = 1,2,\dots,2^{SF}$ and $m = 2^{SF},\dots,2,1$. Applying the Discrete Fourier Transform (DFT) to the sequence $z[k]$ and assuming perfect synchronization, a peak will occur at the bin k that corresponds to the introduced cyclic shift. In order to detect LoRa packets, a specific number of up (or down) chirps are added at the beginning of the transmission as a preamble. Two and a quarter additional chirps are followed for synchronization purposes (in this work only two down chirps are considered as the synchronization symbols).

The aim of the present work is to generate a LoRa packet with an SF of 7 and a BW of 125 kHz, similar to the one represented in Fig. 2 with a simple backscatter modulator front-end circuit. The design is targeted to operate at 2.45 GHz. The proposed circuit can operate with any other value of SF or BW.

III. IQ Impedance Modulator

The circuit used to synthesize and backscatter LoRa packets is shown in Fig. 3 (a). The circuit was simulated and optimized to operate at 2.45 GHz. It consists of two E-PHEMT RF transistors (ATF-54143 [19]) that can generate a set of impedances by changing their bias, allowing to reflect the incident wave with a pre-defined phase value. Since LoRa uses small bandwidths, the frequency at which the phase is changed

(or transistor update) is low. The most important property that the transistors must require is the capability to operate at the backscatter carrier frequency. Due to the low sample rate required, ultra-low power processing units can be attached and operate with the proposed backscatter modulator front-end.

From the previous section, it was shown that any LoRa symbol can be alternatively generated by properly varying the phase of the carrier signal. It is known that phase modulation, in the form of PSK, is an important technique in modern RF systems, and phase modulation can be conveniently achieved, in the form of IQ modulation, by varying the amplitude of the I and Q signals. Hence, by joining the reflected waves from two independent transistors it is possible to add such modulation to the final reflected wave. Here, the quadrature is achieved by inserting a delay of 45 degrees in one of two branches. In the delayed branch, both the incident and the reflected waves experience a delay of 45 degrees, which produces a reflected signal that is in quadrature with the signal produced by the other branch. In this work, a conventional Wilkinson power divider is employed to power divide the incident wave as well as to combine the reflected waves produced by both branches. The losses introduced by the power divider (from power split and insertion loss), will undesirably decrease the value of the reflection coefficient. Nevertheless, space power combining techniques may be considered to avoid those losses, at the expense of at least, one additional antenna. It should be noted that, a sweep on the bias voltage of each branch generates a line of impedances in the Smith Chart, which are converted to a blur by joining the I and Q signals in quadrature, as shown in Fig. 3 (b). All possible synthesized reflection coefficients measured with a grid of 10 mV step (both I and Q voltages), from 0 V to 0.6 V are depicted in Fig. 3 (b). In practice, the circuit was characterized with 1 mV step. The 10 mV representation gives a better visualization of the trend. Parallel open stubs were added at the transistors' drains to shift the response to the center of the Smith Chart. By doing so, a new set of impedances can be achieved whose phases vary 360 degrees, within a constant VSWR circle. Thus, it is possible to create LoRa symbols by properly switching between those points/phases with constant VSWR.

After the circuit's characterization, the reflection coefficients with phases from 0 to 355 degrees with 5-degree step and a VSWR of 1.9 were identified as well as their respective I (Vg1) and Q (Vg2) control voltages. The relation between those phases and voltages is depicted in Fig. 4 and, therefore, every LoRa symbol can be synthesized by following the represented non-linear transformation.

IV. Symbol Coding and Decoding Validation

Based on the relation given in Fig. 4 from the previous section, and also based on the required phase progression given by (7), a single LoRa symbol was synthesized in order to validate the symbol generation process. For this, a two channel Arbitrary Waveform Generator (AWG) was selected to produce the control voltages required for Vg1 and Vg2. Additionally, a Vector Signal Analyzer (VSA) acquires the backscattered

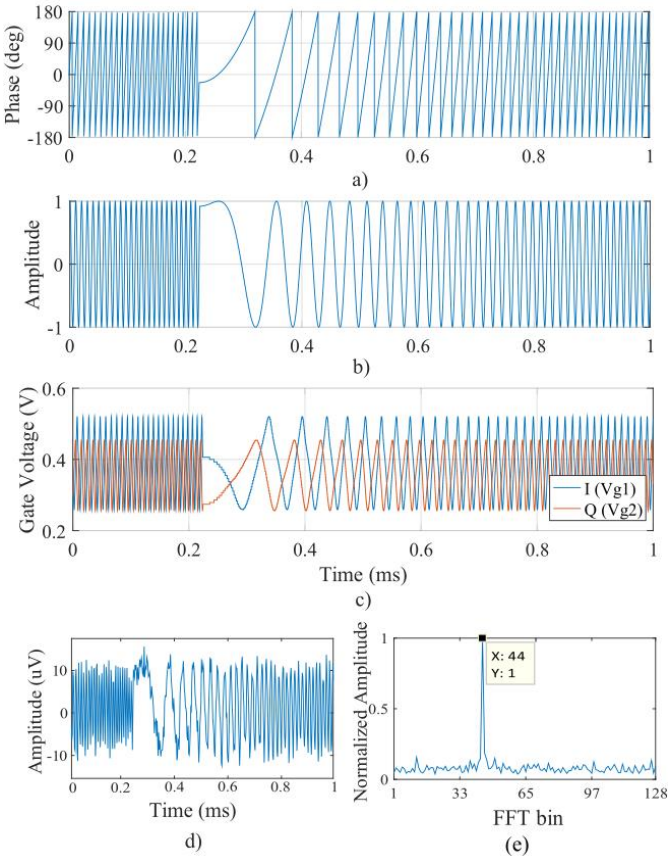

Fig. 5. Generation of one LoRa symbol. (a) Phase progression required to generate the signal; (b) Real component of the complex baseband waveform; (c) I and Q signals required to produce the phase progression for the desired symbol; (d) Real component of the acquired baseband symbol and (e) DFT result.

signal and down-converts it to the complex baseband. The captured complex signal is loaded into the MATLAB and processed. Please note that in a real scenario, the arbitrary waveform generator used to validate our proposed design is replaced by a small microprocessor unit which is intended to operate at the lowest required sampling rate for the lowest power consumption. A future challenge is to employ the control circuit of this modulator. In this work, focus is given to the modulator front-end design and implementation.

Considering symbol index 44 (that is, the result given by (7) cyclically shifted by 44), the phase progression required to generate that symbol is depicted in Fig. 5 (a). In order to obtain a linear frequency modulated signal, the phase of the signal must have a quadratic relation as shown. The presented phase progression will generate a complex signal whose real component is depicted in Fig. 5 (b) and the required control voltages that must be applied to Vg1 and Vg2 to produce the required phase progression are shown in Fig. 5 (c). Finally, the real component of the signal acquired and down-converted by the VSA is shown in Fig. 5 (d) and the symbol estimation in Fig. 5 (e). In this case, the SNR was equal to 9.8 dB and was computed by the following expression,

$$SNR = 10log_{10}\left(\frac{P_{BW} - P_{N,BW}}{P_N}\right) \quad (9)$$

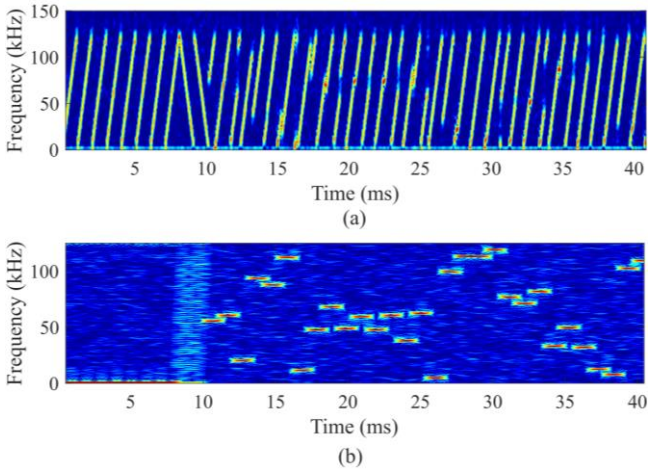

Fig. 6. (a) Measured received LoRa packet spectrogram and (b) its decoding. Only the first 40 symbols out of 12.000 are presented. The packet consists of a preamble of 8 reference symbols, 2 synchronization symbols and 30 data symbols.

where P_{BW} is the total power within the symbol bandwidth (125 kHz), $P_{N,BW}$ the noise power within the symbol bandwidth and P_N the total noise power in the sampled bandwidth. It should be noted that the signal may be sampled at exactly BW Hz, allowing to reduce the total noise power level and thus, enhancing the sensitivity.

A CW signal generator was used to generate the backscatter carrier, and the AWG was loaded with the control bias voltage waveforms, Vg1 and Vg2, previously synthesized. A directional coupler was employed to take a fraction of the reflected wave to feed the VSA. Then, the down-converted I/Q signal was loaded into MATLAB, down-sampled to exactly BW Hz and multiplied by the reference down chirp. Finally, the DFT was applied for symbol decoding.

After symbol coding and decoding validation, a bit stream consisting of 84,000 bits (12,000 symbols) was generated and the respective control voltages, Vg1 and Vg2, were synthesized and loaded to the AWG. A spectrogram of the first 40 symbols received by the VSA are shown in Fig. 6 (a). The represented signal consists of a preamble with 8 reference symbols, 2 synchronization symbols and 30 data symbols. Fig. 6 (b) illustrates the spectrogram from the decoded symbols. After multiplying each symbol with the conjugate of the reference symbol, the preamble, synchronization and transmitted data symbols can be clearly seen. The data symbols are represented by constant frequencies that result from such multiplication. The frequency represents the symbol and the length of the data symbol represents the time that it took to be fully transmitted. The synchronization was performed by delaying the received packet until a maximum occurs at the first DFT bin, for the first 8 preamble symbols.

V. Performance Evaluation

For receiver sensitivity calculations, we require the minimum SNR value so that the information can be decoded without a significant amount of errors, before applying error correction algorithms [20]. LoRa modulation combines Forward Error Correction (FEC) techniques and spread spectrum processing gain to allow high sensitivities. This SNR value depends upon the spreading factor. Lower spreading factor values allow to increase the data rate but will reduce the distance at which the signal can be successfully decoded. On the other hand, higher spreading factor values will increase the OTA time and will in turn, reduce the allowable data rates. Nevertheless, in these situations higher communication distances can be achieved.

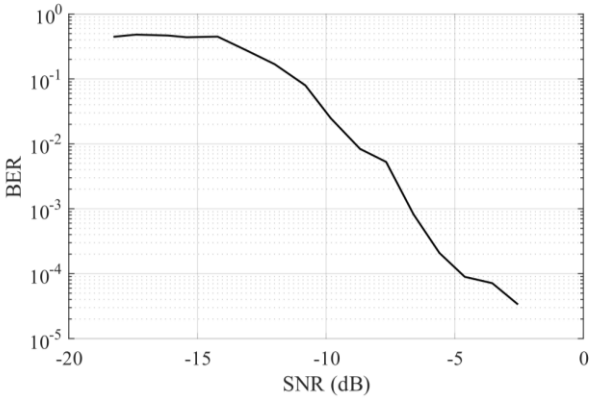

Fig. 7. Measured BER versus received SNR.

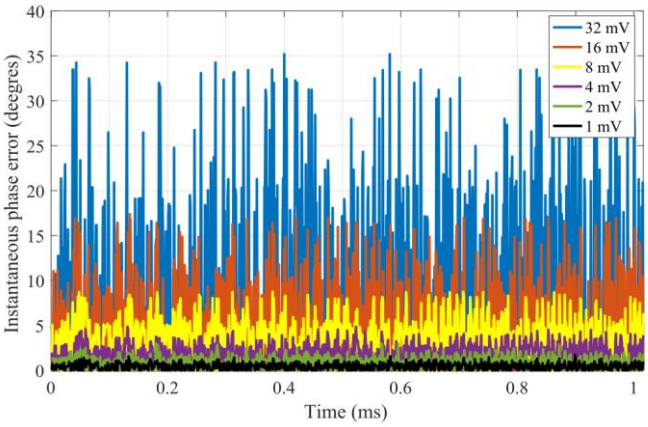

Fig. 8. Instantaneous phase error of one preamble symbol when each sample of the control voltages Vg1 and Vg2 are corrupted with ±1,2,4,8,16 and 32 mV.

In order to evaluate the performance of the proposed LoRa backscatter modulator front-end, cabled as well as OTA tests were conducted as follows.

A. Cabled Measurements

The first experiment was dedicated to evaluate the BER vs SNR. For this, the 12.000 symbols generated before were transmitted several times for each SNR value, sampled by the VSA and processed with MATLAB. The achieved BER was computed by taking the average value of all those measurements and it is plotted in Fig. 7. The achieved results are in accordance with other related work within the literature, with the same spreading factor value [21], [22]. It must be noted that the received signal power level is controlled by setting the appropriate input power level of the backscatter carrier that is fed to the circuit.

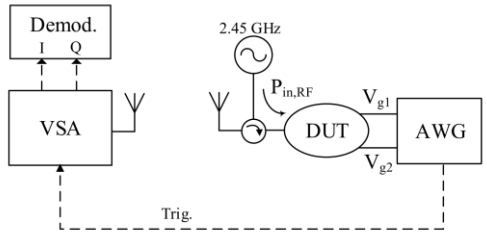

Fig. 9. Block diagram representation of the laboratorial setup used for over-the-air measurements.

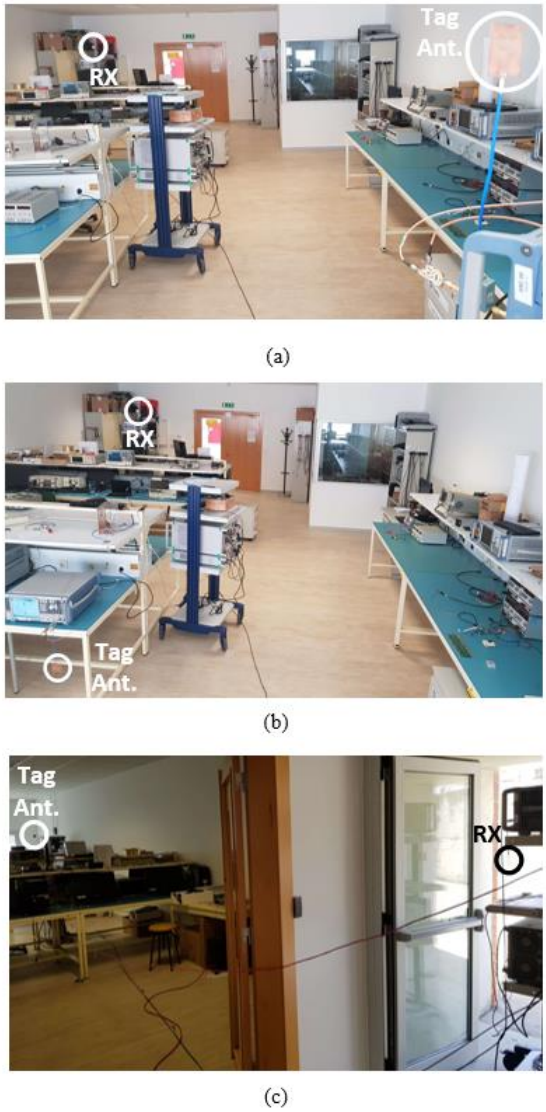

Fig. 10. Scenarios targeted for evaluation. (a) Typical indoor scenario with LoS conditions. The distance between the receiver (VSA) and the device is 10 meters. (b) Desks with laboratorial instruments and other common laboratory hardware in-between the device and the receiver antennas, 7.5 meters. (c) a wall in-between device and receiver, 10 meters.

Additionally, with the same cabled configuration, intentional noise was added to the control voltages that are required to generate a preamble symbol. The aim is to evaluate the required processing unit precision and its robustness against external interferences. Both control voltages were corrupted by random

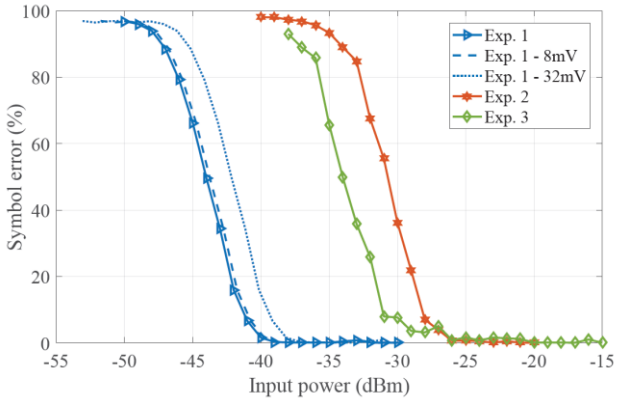

Fig. 11. Symbol error percentage versus backscatter carrier input power level measured for all scenarios. Results for perturbations of ±8 mV and ±32 mV are provided for the first experimental scenario.

perturbations around the nominal value. Perturbations of ±1 mV up to ±32 mV of the nominal value were tested, measured and the instantaneous error between those measurements and the nominal scenario are represented in Fig. 8. The instantaneous phase error is shown to be less than 2 degrees for perturbations of ±1 mV, less than 10 degrees for ±8 mV, and for ±32 mV it can get as high as 35 degrees. It was seen that the BER vs SNR curve, under control bias noise, is exactly the same. However, the backscatter input power must increase to achieve the same SNR. In the following, it will be shown that the impact of a ±8 mV perturbation is almost unnoticeable while ±32 mV starts to produce undesired results.

B. Over-the-Air Measurements

With the laboratorial setup illustrated in Fig. 9, several OTA tests were performed. A 2.45 GHz power source that generates the backscatter carrier is collocated with the proposed device. A circulator redirects the reflected wave to the antenna as shown. The receiver consists of a VSA that down-converts the signal to the complex baseband. Then, the acquired signal is loaded into MATLAB and processed to obtain an estimation of the transmitted information. Two similar single element patch antennas were designed to operate at 2.45 GHz, with an estimated gain of 6 dBi.

Three different indoor scenarios within a laboratory environment were targeted for evaluation and shown in Fig. 10. The aim is to provide information about how much power the device requires from the backscatter carrier to produce a successful transmission. The first, Fig. 10 (a), is a typical indoor scenario with Line-of-Sight (LoS) conditions. An estimation of the distance between the receiver (VSA) and the device is 10 meters. In this particular scenario, intentional perturbations were also added to the control voltages, namely, ±8 mV and ±32 mV. In the second scenario, Fig. 10 (b), the device is positioned close to the floor at roughly 7.5 meters from the receiver. In this situation, there are desks with laboratorial instruments and other common laboratory hardware in-between the device and the receiver antenna. In the third scenario, Fig. 10 (c), the setup is re-positioned in order to account the

effects produced by a wall on the signal's path, with the receiver located 10 meters away from the device.

In all these indoor experiments, 12.000 symbols were transmitted several times for each backscatter carrier input power level (steps of 1 dB) and the percentage of the overall symbol error was computed and shown in Fig. 11. It is shown that in the first scenario, -40 dBm of backscatter carrier input power is required to produce error-free transmissions. Additionally, it is shown that a random perturbation of ±8 mV on the control voltages does not produce noticeable effects, while ±32 mV produces a sensitivity decrease of 2.2 dB. Higher perturbation values require higher backscatter carrier input power to keep the same received SNR. In the second scenario, the non-LoS conditions imposed by the desks determine that the required backscatter carrier input power for error-free transmission is -25 dBm. Finally, due to the wall attenuation, the input power required for error-free transmissions is -26 dBm. It should be noted that the measurements were taken during normal operation of the laboratory and under possible heavy 2.45 GHz Wi-Fi network interference.

Backscatter communications are generally associated with WPT systems. Thus, with the presented approach, it is possible to build a full passive wirelessly powered LoRa backscatter communication device that may operate over larger distances when compared with the conventional SNR needed for ASK, FSK or PSK backscatter modulation systems. Moreover, it is shown that the proposed device has the prominent versatility to backscatter signals compatible with many other standards, thanks to the IQ impedance modulation.

VI. Conclusion

In this paper, an IQ impedance modulator that allows to generate LoRa symbols by reflecting an incident unmodulated carrier was presented. Moreover, the design was validated by generating several LoRa symbols with successful transmissions. Measurements of the un-coded BER vs SNR were conducted. By considering an un-coded BER of 10^{-3}, which can be considered as a reference value, our design requires an SNR of -6.8 dB. One of the main advantages compared to other related circuits is that it is based on a very simple circuit, it employs only two transistors and a power divider. Since LoRa uses small bandwidths, the frequency of the phase change (or transistor update) is low. Due to the low sample rate required, ultra-low power processing units can be attached and operate with this device. By developing the system for 2.45 GHz, it is possible to use the Wi-Fi or 802.15.4 devices (from The Wi-Fi routers and ZigBee hubs) to generate the required RF carriers, since most of those radio transceivers provide access to a special test mode that produces an un-modulated carrier signal.

References

[1] S. J. Thomas, E. Wheeler, J. Teizer, and M. S. Reynolds, "Quadrature amplitude modulated backscatter in passive and semipassive UHF RFID systems," *IEEE Trans. Microw. Theory Tech.*, vol. 60, no. 4, pp. 1175–1182, Feb. 2012.

[2] S. J. Thomas and M. S. Reynolds, "A 96 Mbit/sec, 15.5 pJ/bit 16-QAM modulator for UHF backscatter communication," in *2012 IEEE International Conference on RFID (RFID)*, pp. 185–190, May 2012.

[3] R. Correia, A. Boaventura, and N. B. Carvalho, "Quadrature amplitude backscatter modulator for passive wireless sensors in IoT applications," *IEEE Trans. Microw. Theory Tech.*, pp. 1–8, Feb. 2017.

[4] S. N. Daskalakis, J. Kimionis, A. Collado, G. Goussetis, M. M. Tentzeris, and A. Georgiadis, "Ambient backscatterers using FM broadcasting for low cost and low power wireless applications," *IEEE Trans. Microw. Theory Tech.*, pp. 1–12, Nov. 2017.

[5] V. Liu *et al.*, "Ambient backscatter: wireless communication out of thin air," *SIGCOMM Comput. Commun. Rev.*, vol. 43, no. 4, p. 39, Sep. 2013.

[6] B. Kellogg, A. Parks, S. Gollakota, J. R. Smith, and D. Wetherall, "Wi-Fi backscatter: internet connectivity for RF-powered devices," *SIGCOMM Comput. Commun. Rev.*, vol. 44, no. 4, pp. 607–618, Aug. 2014.

[7] S. N. Daskalakis, R. Correia, G. Goussetis, M. M. Tentzeris, N. B. Carvalho, and A. Georgiadis, "Spectrally efficient 4-PAM ambient FM backscattering for wireless sensing and RFID applications," in *IEEE MTT-S International Microw. Symp. (IMS)*, pp. 266–269, Jun. 2018.

[8] M. Aref and A. Sikora, "Free space range measurements with Semtech LoRa technology," in *2014 2nd Inter. Symp. on Wireless Syst. within the Conf. on Intelligent Data Acquisition and Advanced Computing Syst.*, pp. 19–23, Sep. 2014.

[9] B. Kellogg, V. Talla, J. R. Smith, and S. Gollakot, "PASSIVE WI-FI: Bringing low power to Wi-Fi transmissions," *GetMobile Mob. Comput. Commun.*, vol. 20, no. 3, pp. 38–41, Jan. 2017.

[10] J. F. Ensworth and M. S. Reynolds, "Every smart phone is a backscatter reader: Modulated backscatter compatibility with Bluetooth 4.0 Low Energy (BLE) devices," in *IEEE Int. Conf. on RFID (RFID)*, 2015, pp. 78–85, Apr. 2015.

[11] J. F. Ensworth and M. S. Reynolds, "BLE-Backscatter: Ultralow-power IoT nodes compatible with Bluetooth 4.0 Low Energy (BLE) smartphones and tablets," *IEEE Trans. Microw. Theory Tech.*, vol. 65, no. 9, pp. 3360–3368, Sep. 2017.

[12] V. Iyer, V. Talla, B. Kellogg, S. Gollakota, and J. Smith, "Inter-technology backscatter: towards Internet connectivity for implanted devices," in *Proc. of the 2016 conf. on ACM SIGCOMM*, pp. 356–369, Aug. 2016.

[13] C. Pérez-Penichet, F. Hermans, A. Varshney, and T. Voigt, "Augmenting IoT networks with backscatter-enabled passive sensor tags," in *Proc. of the 3rd Workshop on Hot Topics in Wireless - HotWireless '16*, pp. 23–27, Oct. 2016.

[14] V. Talla, M. Hessar, B. Kellogg, A. Najafi, J. R. Smith, and S. Gollakota, "LoRa Backscatter: Enabling The Vision of Ubiquitous Connectivity," in *Proc. ACM Interact. Mob. Wearable Ubiquitous Technol.*, Vol. 1, no. 3, pp. 105:1-105:24, Sep. 2017.

[15] Y. Peng *et al.*, "PLoRa: A passive long-range data network from ambient LoRa transmissions," in *Proceedings of the 2018 Conference of the ACM Special Interest Group on Data Communication - SIGCOMM '18*, pp. 147–160, Aug. 2018.

[16] R. Correia *et al.*, "Chirp Based Backscatter Modulation," in *IEEE/MTT-S Int. Microw. Symp. (IMS)*, pp. 279-282, Jun. 2019.

[17] Microsemi, IGLOO nano Low Power Flash FPGAs with Flash*Freeze Technology, Revision 27, DS0110.

[18] A. Varshney, C. Pérez-Penichet, C. Rohner, and T. Voigt, "LoRea: A backscatter architecture that achieves a long communication range," in *Proc. ACM Embedded Netw. Sensor Syst. (SenSys)*, p. 50, Nov. 2017.

[19] Agilent ATF-54143 Low Noise Enhancement Mode Pseudomorphic HEMT in a Surface Mount Plastic Package. Datasheet, https://docs.broadcom.com/docs/AV02-0488EN

[20] SX1272/3/6/7/8:LoRaModem (2013). https://www.semtech.com/uploads/documents/LoraDesignGuide_STD.pdf

[21] T. Elshabrawy and J. Robert, "Closed-form approximation of LoRa modulation BER performance," *IEEE Comm. Lett.*, vol. 22, no. 9, pp. 1778-1781, Sept. 2018.

[22] D. Croce, M. Gucciardo, S. Mangione, G. Santaromita, and I. Tinnirello, "Impact of LoRa imperfect orthogonality: analysis of link-level performance," *IEEE Comm. Lett.*, vol. 22, no. 4, pp. 796-799, Apr. 2018.

Daniel Belo received his M.Sc. degree in electronics and telecommunications engineering in 2014 from University of Aveiro, Aveiro, Portugal. He is a researcher at Instituto de Telecomunicações since 2013 and his main areas of interest are microwave electronic circuits, wireless power transfer systems and analogue/digital control. He is currently working towards the Ph.D. degree at University of Aveiro.

Ricardo Correia (GS'15) received the M.Sc. degree in electronics and telecommunications engineering from the University of Aveiro, Aveiro, Portugal, in 2009, and the Ph.D. degree in electrical engineering at University of Aveiro in 2019. He was an Automation and Electrical Engineer and a Researcher in embedded systems and signal processing. He is currently a Researcher at Sinuta SA. – Estarreja, Aveiro where he works on transmission and reception system of electronically oriented signals for next generation satellite constellations. He is also a collaborator at the Institute of Telecommunications, University of Aveiro. His current research interests include wireless power transfer, energy harvesting, wireless passive sensors for space applications, and low power communications. Mr. Correia is a member of the IEEE Microwave Theory and Techniques Society. He is also a Reviewer for the IET Microwaves, Antennas and Propagation, Wireless Power Transfer Journal and the IEEE TRANSACTIONS ON MICROWAVE THEORY AND TECHNIQUES. He was a recipient of the 2016 URSI/ANACOM Prize awarded by the URSI Portuguese Section and Portuguese National Authority of Communications.

Yuan Ding received his Bachelor's degree from Beihang University (BUAA), Beijing, China, in 2004, received his Master's degree from Tsinghua University, Beijing, China, in 2007, and received his Ph.D. degree from Queen's University of Belfast, Belfast, UK, in 2014, all in Electronic Engineering.

He was a radio frequency (RF) Engineer in Motorola R&D Centre (Beijing, China) from 2007 to 2009, before joining Freescale Semiconductor Inc. (Beijing, China) as an RF Field Application Engineer, responsible for high power base-station amplifier design, from 2009 to 2011. He is now an Assistant Professor at the Institute of Sensors, Signals and Systems (ISSS) in Heriot-Watt University, Edinburgh, UK. His research interests are in antenna array, physical layer security, backscattering communication and 5G related areas.

Dr. Ding was the recipient of the IET Best Student Paper Award at LAPC 2013 and the recipient of the Young Scientists Awards in General Assembly and Scientific Symposium (GASS), 2014 XXXIst URSI.

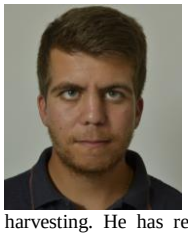

Spyridon Nektarios Daskalakis (S'12) was born in Heraklion, Greece in 1991. He received with excellence his Engineering Diploma and the M.Sc. in Electrical and Computer Engineering from Technical University of Crete (TUC) in 2014 and 2016, respectively. He is currently working toward the PhD degree in School of Engineering and Physical Sciences from Heriot-Watt university, Edinburgh UK. His current research interests include low-power, low-cost wireless sensor networks and energy harvesting. He has received fellowship award by the Clinton Global Initiative University 2014 (USA), the Onassis Foundation (graduate studies 2015/16 scholarship), the Lloyds Register Foundation (LRF) and the International Consortium in Nanotechnology (ICON). He was a recipient for two short-term scientific mission grands from COST Action IC1301 WiPE in School of Electrical and Computer Engineering, Georgia Institute of Technology, Atlanta in 2016, and the Centre Tecnologic de Telecomunicacions de Catalunya, Barcelona in 2015. He is also a recipient of MTT-S Graduate Fellowship for 2019 from IEEE Microwave Theory and Techniques Society and recipient of 1st and 2nd Year Postgraduate Research Prizes from Heriot-Watt University.

George Goussetis (S 99, M 02, SM 12) received the Diploma degree in Electrical and Computer Engineering from the National Technical University of Athens, Greece, in 1998, and the Ph.D. degree from the University of Westminster, London, UK, in 2002. In 2002 he also graduated B.Sc. in physics (first class) from University College London (UCL), UK.

In 1998, he joined the Space Engineering, Rome, Italy, as RF Engineer and in 1999 the Wireless Communications Research Group, University of Westminster, UK, as a Research Assistant. Between 2002 and 2006 he was a Senior Research Fellow at Loughborough University, UK. He was a Lecturer (Assistant Professor) with Heriot-Watt University, Edinburgh, UK between 2006 and 2009 and a Reader (Associate Professor) with Queen's University Belfast, UK, between 2009 and 2013. In 2013 he joined Heriot-Watt as a Reader and was promoted to Professor in 2014, where he currently directs the Institute of Sensors Signals and Systems. He has authored or co-authored over 500 peer-reviewed papers five book chapters one book and four patents. His research interests are in the area of microwave and antenna components and subsystems.

Dr. Goussetis has held a research fellowship from the Onassis foundation in 2001, a research fellowship from the UK Royal Academy of Engineering between 2006-2011 and European Marie-Curie experienced researcher fellowships in 2011-12 and again in 2014-17. He is the co-recipient of the 2011 European Space Agency young engineer of the year prize, the 2011 EuCAP best student paper prize, the 2012 EuCAP best antenna theory paper prize and the 2016 Bell Labs prize. He has served as Associate Editor to the IEEE Antennas and Wireless Propagation Letters.

Apostolos Georgiadis received the Ph.D. in electrical engineering from the University of Massachusetts, USA. He has held positions as systems engineer in the industry in USA and as senior researcher and group leader in microwave subsystems in Spain. In 2016-2017 he was Associate Professor at Heriot-Watt University, UK and presently he is a patent examiner at the European Patent Office. He has authored more than 200 papers in peer-reviewed journals and international conferences. His research interests include energy harvesting and wireless power transfer, RFID technology, active antennas, inkjet and 3D-printed electronics. His research has received several best paper awards and the 2016 Bell Labs Prize. He was Fulbright Fellow and EU Marie Curie Global Fellow. He was Associate Editor of the IET Microwaves Antennas and Propagation and the IEEE Microwave and Wireless Components Letters journals. He co-founded and was Editor-in-Chief of the Wireless Power Transfer Journal. He was Distinguished Lecturer of the IEEE Council on RFID. He is URSI Fellow and 2017-2020 Chair of URSI Commission D.

Nuno Borges Carvalho (S'97–M'00–SM'05-F'15) was born in Luanda, Angola, in 1972. He received the Diploma and Doctoral degrees in electronics and telecommunications engineering from the University of Aveiro, Aveiro, Portugal, in 1995 and 2000, respectively.

He is currently a Full Professor and a Senior Research Scientist with the Institute of Telecommunications, University of Aveiro and an IEEE Fellow. He coauthored Intermodulation in Microwave and Wireless Circuits (Artech House, 2003), Microwave and Wireless Measurement Techniques (Cambridge University Press, 2013) and White Space Communication Technologies (Cambridge University Press, 2014). He has been a reviewer and author of over 200 papers in magazines and conferences. He is the Editor in Chief of the Cambridge Wireless Power Transfer Journal, an associate editor of the IEEE Microwave Magazine and former associate editor of the IEEE Transactions on Microwave Theory and Techniques and IET Microwaves Antennas and Propagation Journal.

He is the co-inventor of six patents. His main research interests include software-defined radio front-ends, wireless power transmission, nonlinear distortion analysis in microwave/wireless circuits and systems, and measurement of nonlinear phenomena. He has recently been involved in the design of dedicated radios and systems for newly emerging wireless technologies.

Dr. Borges Carvalho is a member of the IEEE MTT ADCOM, the past-chair of the IEEE Portuguese Section, MTT-20 and MTT-11 and also belong to the technical committees, MTT-24 and MTT-26. He is also the vice-chair of the URSI Commission A (Metrology Group). He was the recipient of the 1995 University of Aveiro and the Portuguese Engineering Association Prize for the best 1995 student at the University of Aveiro, the 1998 Student Paper Competition (Third Place) of the IEEE Microwave Theory and Techniques Society (IEEE MTT-S) International Microwave Symposium (IMS), and the 2000 IEE Measurement Prize.

He is a Distinguished Microwave Lecturer for the IEEE Microwave Theory and Techniques Society.